

Molecular dynamics study of H<sub>2</sub> dissociation on H-covered Pd(100)A. Lozano,<sup>1</sup> A. Groß,<sup>2</sup> and H. F. Busnengo<sup>1</sup><sup>1</sup>*Instituto de Física de Rosario, Consejo Nacional de Investigaciones Científicas y Técnicas (CONICET) and Universidad Nacional de Rosario, Av. Pellegrini 250, 2000 Rosario, Argentina*<sup>2</sup>*Institute of Theoretical Chemistry, University of Ulm, 89069 Ulm, Germany*

(Received 1 February 2010; published 2 March 2010)

We employ classical molecular dynamics calculations based on density-functional theory molecule-surface interaction potentials to study H-coverage effects on H<sub>2</sub> dissociative adsorption on Pd(100). In contrast with one of the basic assumptions of the widely used Langmuir model, we have found that a single isolated H-vacancy is enough to spontaneously dissociate low-energy H<sub>2</sub> molecules on H-covered Pd(100). We also show that for a given initial coverage (e.g.,  $\Theta=1/2$ ), the dissociative adsorption probability of low-energy H<sub>2</sub> molecules can vary by a factor of five depending on the particular arrangement of the H adatoms on the surface.

DOI: 10.1103/PhysRevB.81.121402

PACS number(s): 68.43.-h, 82.65.+r, 34.35.+a

Dissociative adsorption of H<sub>2</sub> is a prerequisite for heterogeneous catalytic hydrogenation, H storage, and many other technologically relevant processes (see, e.g., Ref. 1 and references therein). This has motivated many theoretical studies, most of which have been focused on the interaction of H<sub>2</sub> with clean metal surfaces. However, under conditions of practical interest, adsorption takes place on partially covered surfaces.

Experimentally, coverage effects have been traditionally investigated by measuring the dissociative adsorption probability,  $P_{\text{diss}}$ , by differentiation of the coverage,  $\Theta$  (i.e., the number of adsorbates per topmost layer surface atom), as a function of exposure. Thus,  $P_{\text{diss}}(\Theta)$  represents an average over all the possible local arrangements of adatoms (consistent with  $\Theta$ ) at the experimental conditions which make difficult the comparison with theory. Such  $P_{\text{diss}}(\Theta)$  curves are always ultimately rationalized (irrespective of the surface structure) using the Langmuir model which assumes that two (or more generally  $n \geq 2$ ) nearest-neighbor (NN) empty adsorption sites are required for a diatomic molecule to dissociate [so,  $\bar{p}(\Theta) = P_{\text{diss}}(\Theta) / P_{\text{diss}}(\Theta=0) = (1-\Theta)^n$ ] (Ref. 2) or introducing additional hypotheses to account for precursor mediated adsorption.<sup>3</sup> For H<sub>2</sub>/Pd(100) it was found that  $\bar{p}(\Theta) > (1-\Theta)$ ,<sup>4</sup> whereas for H<sub>2</sub>/Pd(111)  $\bar{p}(\Theta) < (1-\Theta)$ .<sup>5,6</sup> In other words, H adatoms passivate Pd(111) more *efficiently* than Pd(100). Obviously, this surface structure effect cannot be understood through the simple empirical models mentioned above.

Low-temperature scanning tunneling microscopy (STM) is a complementary tool allowing to measure the sticking coefficient for surface *patches* with particular arrangements of adatoms and vacancies. This technique has been applied for the first time to H<sub>2</sub>/Pd(111).<sup>7,8</sup> It was found that on a H-covered Pd(111) surface offering two nearest-neighbor vacancies (NNVs)  $P_{\text{diss}}$  is negligible, and even on aggregates of three, four, and five NNV,  $P_{\text{diss}}$  is much smaller than on a similar *patch* of clean Pd(111).<sup>7</sup> This has motivated various theoretical investigations based on density-functional theory (DFT) calculations<sup>9</sup> as well as *Ab Initio* Molecular Dynamics (AIMD) simulations.<sup>10</sup> The extremely low reactivity of two NNV in H-covered Pd(111) was attributed to the fact that at least one Pd atom with no direct interaction with preadsorbed

H atoms is required to act as an active dissociation site for Pd(111).<sup>9</sup>

To understand the origin of the surface structure dependence of H-coverage effects for H<sub>2</sub>/Pd, we have investigated H<sub>2</sub>/Pd(100) by using classical molecular dynamics (MD) calculations based on DFT molecule-surface interaction potentials. We show that, in contrast with the basic assumption of the Langmuir model, a single isolated H-vacancy is enough to spontaneously dissociate H<sub>2</sub> on H-covered Pd(100). Together with previous results for H<sub>2</sub>/Pd(111),<sup>7-10</sup> our findings are in line with the surface structure dependence of H-coverage effects for H<sub>2</sub>/Pd obtained in experiments.<sup>4-6</sup> We have also found that even for a given coverage ( $\Theta=1/2$ ), at low energies  $P_{\text{diss}}$  can vary by a factor of 5 depending on the particular arrangement of the adatoms on Pd(100) which highlights the limitations of simple models based only on the knowledge of the average surface coverage  $\Theta$ . We expect our surprising predictions will stimulate further STM investigations of H-coverage effects for H<sub>2</sub>/Pd(100).

For H/Pd(100), the DFT predictions (present work and Refs. 11–14) with respect to the hollow site as the energetically most favorable adsorption site and its corresponding adsorption energy are both in good agreement with experiments.<sup>4,15,16</sup> We have computed  $P_{\text{diss}}$  as a function of the molecular impact energy,  $E_i$ , for all the arrangements of adatoms shown in Fig. 1. These structures will be referred to as (a) Pd(100)-H<sub>1/4</sub>, (b) Pd(100)-H<sub>1/2</sub>(1×2), (c) Pd(100)-H<sub>1/2c</sub>(2×2), and (d) Pd(100)-H<sub>3/4</sub>. Already for Pd(100)-H<sub>1/4</sub> every topmost-layer Pd atom is in direct interaction with one adatom. For Pd(100)-H<sub>1/4</sub> and Pd(100)-H<sub>1/2</sub>(1×2), there are bridge sites in the middle of

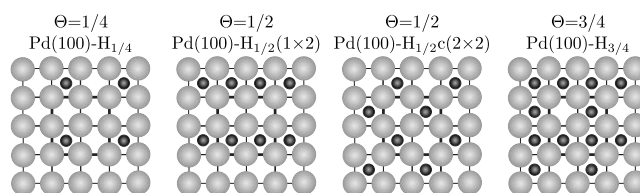


FIG. 1. Possible arrangements of H adatoms (black circles) within a (2×2) Pd(100) unit cell indicated with thick lines.

two NN empty hollow sites. In contrast, on Pd(100)-H<sub>1/2</sub>c(2×2) there exist only next-nearest-neighbor (NNN) empty hollow sites and on Pd(100)-H<sub>3/4</sub>, empty hollow sites, *h*, are *isolated* surrounded by occupied hollow sites, *ho*. In what follows, bridge sites that are NN (NNN) of at least one *ho* site will be referred to as *b*<sub>1</sub>(*b*<sub>2</sub>).

DFT calculations were carried out with the Vienna *Ab initio* Simulation Package (VASP) (Refs. 17–20) that uses a plane wave basis set for the electronic orbitals. Electronic exchange and correlation was described within the generalized gradient approximation proposed by Perdew and Wang.<sup>21</sup> The Pd(100) surface has been represented by a four-layer slab and the interaction between valence electrons and the atomic cores was described within the projected augmented wave method<sup>22</sup> implemented in VASP.<sup>23</sup> The energy cutoff was 350 eV and electronic smearing was introduced within the Metfessel and Paxton scheme with  $N=1$  and  $\sigma=0.2$  eV.<sup>24</sup> We have used a  $5 \times 5 \times 1$   $\mathbf{k}$  points grid and all the calculations were spin restricted. Various tests showed that our DFT total energies are well converged; errors being smaller than the typical ones of the interpolation schemes used to obtain continuous representations of the potential-energy surfaces (PESs) (see below). We have first optimized the distance between the Pd layers and the height of the H overlayer. Then, to compute the H<sub>2</sub>/Pd(100)-H PESs, Pd and H adatoms were kept fixed in their optimum positions. Throughout this work, ( $X, Y, Z$ ) are the Cartesian coordinates of the molecular center of mass,  $r$  is the H-H distance,  $\theta$  and  $\phi$  are, respectively, the polar and azimuthal angle of the internuclear vector and the reference energy level ( $V=0$ ) always corresponds to H<sub>2</sub> at equilibrium ( $r=r_{eq}=0.75$  Å) far from the surface.

Figure 2 shows 2D( $Z, r$ ) cuts of the PESs of H<sub>2</sub> interacting with: (a) clean Pd(100) (Ref. 25), (b) Pd(100)-H<sub>1/4</sub>, (c) Pd(100)-H<sub>1/2</sub>(1×2), (d) Pd(100)-H<sub>1/2</sub>c(2×2), and (e) Pd(100)-H<sub>3/4</sub>. For  $\Theta=0$ , nonactivated dissociation pathways do exist on top (*t*) and bridge sites whereas dissociation over *h* sites is slightly activated. For  $\Theta=1/4$ , the presence of the H adatoms introduces a large repulsion for the incoming molecule close to *ho* sites. This eliminates the nonactivated dissociation pathways on *b*<sub>1</sub> sites. Though on *t* sites the PES is much less affected, dissociative adsorption also becomes slightly activated. In contrast, 2D( $Z, r$ ) cuts of the PES on *h* and *b*<sub>2</sub> sites for Pd(100)-H<sub>1/4</sub> are barely modified with respect to the ones for clean Pd(100) on *h* and *b* sites, respectively. For H<sub>2</sub>/Pd(100)-H<sub>1/2</sub>(1×2), 2D( $Z, r$ ) nonactivated pathways still exist on *b*<sub>2</sub> sites. However, for Pd(100)-H<sub>1/2</sub>c(2×2) and Pd(100)-H<sub>3/4</sub>, there is no longer *b*<sub>2</sub> sites within the (2×2) unit cell and all 2D( $Z, r$ ) non activated dissociation pathways are definitively lost.<sup>26</sup>

The effect of the H adatoms on the H<sub>2</sub>/Pd(100)-H<sub>1/4</sub> PES can be accurately accounted for by introducing a pairwise potential,  $V_{H-H}$ , between the atoms of H<sub>2</sub> and the adatoms. Thus, we have built the PES for  $\Theta=1/4$ ,  $V_{\Theta=1/4}^{6D}$ , using the expression

$$V_{\Theta=1/4}^{6D} = V_0^{6D} + \sum_i \sum_{j=1,2} V_{H-H}(\rho_{ij}), \quad (1)$$

where  $V_0^{6D}$  is the 6D PES for clean Pd(100) (Ref. 25) obtained by using the corrugation reducing procedure (CRP).<sup>27</sup>

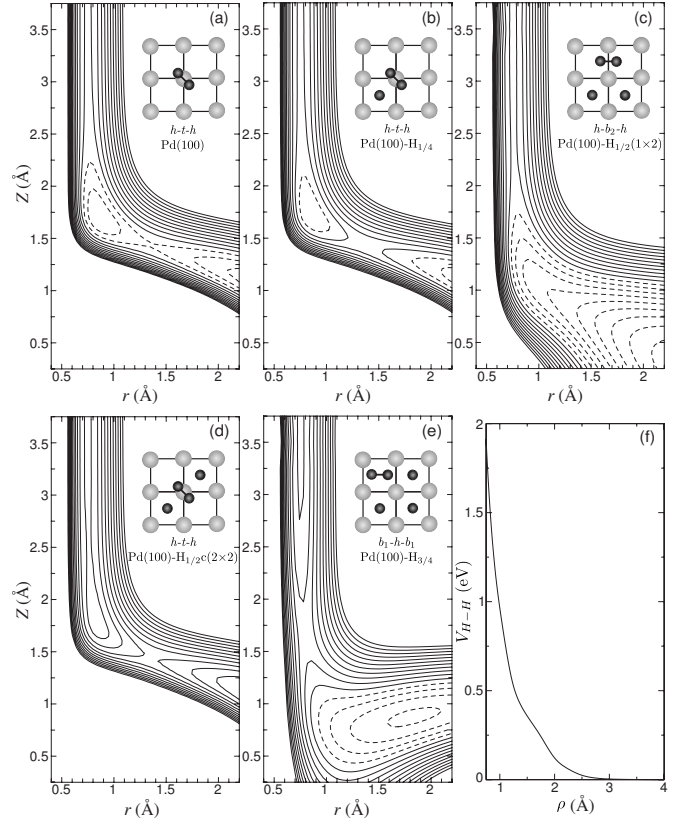


FIG. 2. [(a)–(e)] 2D( $Z, r$ ) cuts of the PESs of H<sub>2</sub> interacting with H-covered Pd(100). Intervals between contours: 0.1 eV. Dashed lines: negative values. Full lines: positive values. Thick line:  $V=0$  eV. (f)  $V_{H-H}(\rho)$  (see text).

In Eq. (1),  $\rho_{ij}$  is the distance between the  $i$ th H adatom and the  $j$ th atom of H<sub>2</sub> (periodic images of the adatoms are included in the sum). We have used the  $V_{H-H}$  potential that minimizes the deviations with respect to DFT energies  $<0.6$  eV [i.e., near the 2D( $Z, r$ ) minimum energy paths] for H<sub>2</sub> parallel to Pd(100)-H<sub>1/4</sub> and with its center of mass on the *ho* site.<sup>26</sup> Figure 2(f) shows the resulting repulsive  $V_{H-H}(\rho)$  potential that becomes almost negligible for  $\rho > 2.8$  Å (i.e., the NN Pd-Pd distance).

For  $\Theta=1/2$ , Eq. (1) is still qualitative adequate but predicts interaction energies slightly too low compared with the DFT results. So, the PESs for H<sub>2</sub>/Pd(100)-H<sub>1/2</sub>(1×2) and H<sub>2</sub>/Pd(100)-H<sub>1/2</sub>c(2×2), hereafter referred to as  $V_{1 \times 2}^{6D}$  and  $V_{c(2 \times 2)}^{6D}$ , respectively, were interpolated by using the *standard* CRP (Ref. 27) but subtracting not only the H-clean Pd(100) potential but also the sum of pairwise potentials  $V_{H-H}$  of Eq. (1), in order to reduce the corrugation of the DFT data. Finally, for  $\Theta=3/4$  we also employed Eq. (1) but using  $V_{c(2 \times 2)}^{6D}$  instead of  $V_0^{6D}$ . We have carefully checked that this procedure provides accurate continuous representations of the PESs for H<sub>2</sub> interacting with all the surfaces shown in Fig. 1.<sup>26</sup>

Figure 3 shows quasiclassical (QC) results of  $P_{\text{diss}}(E_i)$  for H<sub>2</sub>( $\nu=0, J=0$ ) impinging at normal incidence on Pd(100) at the initial coverages:  $\Theta=1/4, 1/2$ , and  $3/4$ . For comparison, we have also included classical results for clean Pd(100) taken from Ref. 25. For each  $E_i$  we have integrated 5000

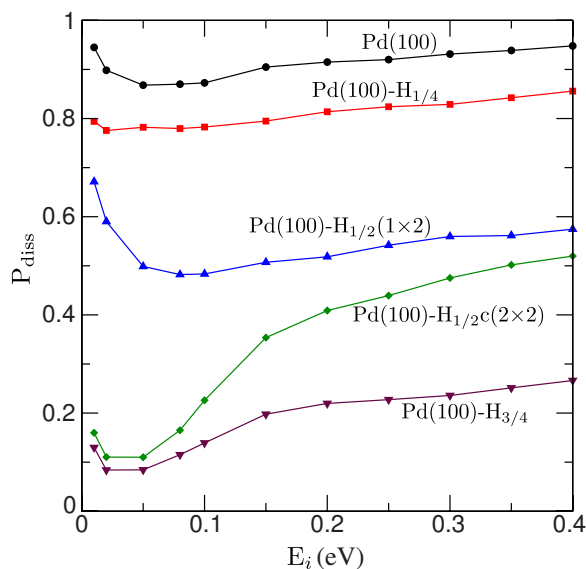


FIG. 3. (Color online) Quasiclassical H<sub>2</sub> dissociative adsorption probability on H-covered Pd(100) for  $\Theta=1/4$ ,  $1/2$ , and  $3/4$ , as a function of  $E_i$ . Classical results for clean Pd(100), taken from Ref. 25.

trajectories and considered that dissociation takes place whenever  $r$  reaches  $2.25 \text{ \AA}$  and  $dr/dt > 0$ . As expected,  $P_{\text{diss}}$  decreases when  $\Theta$  increases. The most striking result is that dissociative adsorption is non activated on Pd(100)-H<sub>3/4</sub>, in spite of the fact that there are only *isolated h* sites on the surface. Actually, the fact that at low energies,  $P_{\text{diss}} \sim 0.15$  on Pd(100)-H<sub>1/2c</sub>(2×2) despite of the absence of NNVs is also unexpected. The existence of nonactivated dissociation pathways on Pd(100)-H<sub>1/2c</sub>(2×2) and Pd(100)-H<sub>3/4</sub> was further confirmed by using the nudged elastic band (NEB) method<sup>28</sup> (directly coupled to DFT calculations) starting from an initial sequence of images taken from one of the reactive trajectories for  $E_i=10 \text{ meV}$  (further details will be given elsewhere<sup>26</sup>). The reaction pathways (RPs) coming out from the NEB calculations for Pd(100)-H<sub>1/2c</sub>(2×2) and Pd(100)-H<sub>3/4</sub>, which are very similar to each other, are shown in Fig. 4 as well as some molecular configurations along the RP for  $\Theta=3/4$ . First, the molecule approaches parallel to the surface on a *t* site (panel b-A), then it tilts and simultaneously goes to a site between *t* and *h* (panels b-B and b-C), and finally dissociates parallel to the surface with its center of mass close to a *h* site with the internuclear vector pointing toward *b*<sub>1</sub> sites (panel b-D). Additional NEB calculations for a 3×3 unit cell (not shown) with a single vacancy (i.e.,  $\Theta=8/9$ ) also give a very similar nonactivated RP.

At low coverages ( $\Theta=0$  and  $\Theta=1/4$ ) only a small fraction of trajectories become dynamically trapped. Thus, dissociative adsorption is essentially a direct process (still most of the trapped molecules dissociate). At low energies, the fraction of dynamically trapped trajectories increases when  $\Theta$  increases. For Pd(100)-H<sub>1/2</sub>(1×2), the efficacy of dynamic trapping to promote dissociation is also high and  $\sim 80\%$  of the dissociation events takes place after dynamic trapping. However, on Pd(100)-H<sub>1/2c</sub>(2×2) and on

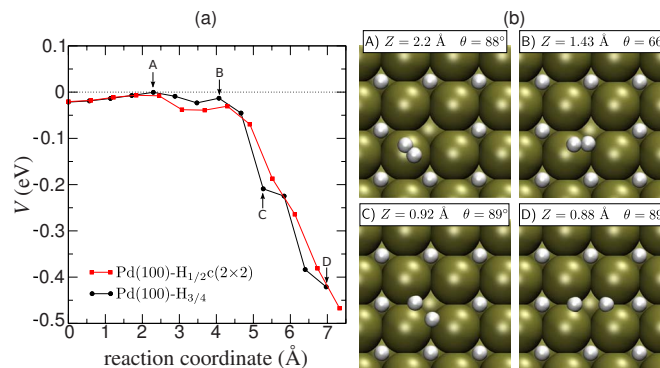


FIG. 4. (Color online) (a) Nonactivated RPs for H<sub>2</sub> dissociation on Pd(100)-H<sub>1/2c</sub>(2×2) and Pd(100)-H<sub>3/4</sub>. (b) Some molecular configurations along the RP for H<sub>2</sub>/Pd(100)-H<sub>3/4</sub>.

Pd(100)-H<sub>3/4</sub> there are even more dynamically trapped molecules, but this indirect mechanism becomes less effective as dissociation promoter because of the large suppression of energetically accessible dissociation pathways: a large fraction of trapped trajectories are finally reflected. This is why the most pronounced nonmonotonic behavior of  $P_{\text{diss}}(E_i)$  is found on Pd(100)-H<sub>1/2</sub>(1×2). Following the evolution of reactive trajectories at low energies, we observed that for  $\Theta=0$  the majority of the molecules dissociate over *b* and *t* sites. On Pd(100)-H<sub>1/4</sub> and Pd(100)-H<sub>1/2</sub>(1×2), most of dissociation events take place near *b*<sub>2</sub> sites with H atoms dissociating toward NN *h* sites. In contrast, on Pd(100)-H<sub>1/2c</sub>(2×2) and Pd(100)-H<sub>3/4</sub>, dissociation events can only take place for those molecules that approach parallel to the surface around *t* sites (up to  $Z \sim 1.75 \text{ \AA}$ ) and are then redirected toward *h* sites (changing the tilt angle  $\theta$ ), so avoiding the activation barriers present in the entrance channel on *h* sites [Fig. 2(e)]. Thus, the reduction in  $P_{\text{diss}}$  on Pd(100)-H<sub>1/2c</sub>(2×2) with respect to Pd(100)-H<sub>1/2</sub>(1×2) by a factor of  $\sim 5$  at low energies, is essentially due to a strong suppression of direct dissociation because of the disappearance of *b*<sub>2</sub> sites on which dissociation is more straightforward. In other words, two NNVs largely enhance direct dissociation in line with the Langmuir model. Still, H<sub>2</sub> dissociative adsorption remains a non activated process even on a single vacancy on H-covered Pd(100). Interestingly, the very different values of  $P_{\text{diss}}$  for surface *patches* with H adatoms forming *c*(2×2)- and (1×2)-like structures might be detected in low-temperature STM experiments.<sup>7,8</sup> In connection with this, it is important to mention that the energy per 2×2 unit cell of Pd(100)-H<sub>1/2c</sub>(2×2) is  $\sim 0.09 \text{ eV}$  lower than for Pd(100)-H<sub>1/2</sub>(1×2), in line with the *c*(2×2) structure observed in low-energy electron diffraction experiments for H/Pd(100) for  $\Theta=1/2$ .<sup>4</sup>

It might be argued that our conclusions could change if energy transfer with the surface is allowed. To check this, we used the AIMD approach previously employed in Ref. 10 with the uppermost two layers of the Pd substrate allowed to move to calculate  $P_{\text{diss}}$  for Pd(100)-H<sub>1/2c</sub>(2×2) and Pd(100)-H<sub>3/4</sub>. For each system we ran 200 classical (without initial vibrational zero-point energy, ZPE) trajectories with  $E_i=0.1 \text{ eV}$  and the surface atoms initially at rest, i.e., for a surface temperature,  $T_s=0 \text{ K}$ . We obtained  $P_{\text{diss}}=0.25$  for

Pd(100)-H<sub>1/2</sub>c(2×2) and 0.12 for Pd(100)-H<sub>3/4</sub>. Together with  $P_{\text{diss}}=0.62$  already reported for Pd(100)-H<sub>1/2</sub>(1×2),<sup>10</sup> these results agree quite well with the ones shown in Fig. 3 but it must be considered that higher values would be obtained taking into account the initial ZPE in the AIMD calculations, due to vibrational softening.<sup>26</sup> Thus, AIMD calculations predict a larger reactivity mainly because surface recoil facilitates the molecular trapping for  $T_s=0$  K. Practically, all of these trapped molecules eventually dissociate rather than desorb. This means that the results obtained within the rigid substrate approximation can be regarded as a lower bound for  $P_{\text{diss}}$  for  $T_s=0$  K. Still, our AIMD results unambiguously confirm the main conclusions of the analysis of the rigid surface dynamics.

Furthermore, using a larger 3×3 surface unit cell with  $\Theta=5/9$ , 6/9, and 7/9, it was observed that when H<sub>2</sub> dissociates at a single H vacancy, an exchange-like mechanism allows the diffusion of one of the H atoms until it finds an empty adsorption site.<sup>10</sup> If there are no additional empty hol-

low sites near the one where dissociation takes place, the *extra* H might also end adsorbed in an octahedral  $O_h$  subsurface site.<sup>14</sup>

To summarize, we have carried out MD simulations to investigate H-coverage effects on dissociative adsorption of H<sub>2</sub> on Pd(100). In contrast with one of the basic assumptions of the widely used Langmuir model, we find that an isolated H-vacancy is enough to spontaneously dissociate H<sub>2</sub> on H-covered Pd(100). We have also found that for a given surface coverage,  $\Theta$ , the dissociative adsorption probability at low energies can vary by a factor of five depending on the particular arrangement of H adatoms. We hope this will stimulate further experimental studies for H<sub>2</sub>/Pd(100) with techniques that allow to estimate the sticking probability on surface *patches* with particular arrangements of adatoms.

The work of A.L and H.F.B was supported by CONICET-Argentina (project N° PIP 5248) and ANPCyT-Argentina (project N° PICT 33595).

- 
- <sup>1</sup>G. J. Kroes, A. Groß, E. J. Baerends, M. Scheffler, and D. A. McCormack, *Acc. Chem. Res.* **35**, 193 (2002).  
<sup>2</sup>I. Langmuir, *J. Am. Chem. Soc.* **38**, 1145 (1916).  
<sup>3</sup>P. Kisliuk, *J. Phys. Chem. Solids* **3**, 95 (1957).  
<sup>4</sup>R. J. Behm, K. Christman, and G. Ertl, *Surf. Sci.* **99**, 320 (1980).  
<sup>5</sup>T. Engel and H. Kuipers, *Surf. Sci.* **90**, 162 (1979).  
<sup>6</sup>M. P. Kiskinova and G. M. Bliznakov, *Surf. Sci.* **123**, 61 (1982).  
<sup>7</sup>T. Mitsui, M. K. Rose, E. Fomin, D. F. Ogletree, and M. Salmeron, *Nature (London)* **422**, 705 (2003).  
<sup>8</sup>T. Mitsui, M. K. Rose, E. Fomin, D. F. Ogletree, and M. Salmeron, *Surf. Sci.* **540**, 5 (2003).  
<sup>9</sup>N. Lopez, Z. Lodziana, F. Illas, and M. Salmeron, *Phys. Rev. Lett.* **93**, 146103 (2004).  
<sup>10</sup>A. Groß and A. Dianat, *Phys. Rev. Lett.* **98**, 206107 (2007).  
<sup>11</sup>S. Wilke, D. Hennig, and R. Löber, *Phys. Rev. B* **50**, 2548 (1994).  
<sup>12</sup>A. Eichler, J. Hafner, and G. Kresse, *J. Phys.: Condens. Matter* **8**, 7659 (1996).  
<sup>13</sup>W. Dong, V. Ledentu, P. Sautet, A. Eichler, and J. Hafner, *Surf. Sci.* **411**, 123 (1998).  
<sup>14</sup>S. C. Jung and M. H. Kang, *Phys. Rev. B* **72**, 205419 (2005).  
<sup>15</sup>F. Besenbacher, I. Stensgaard, and K. Mortensen, *Surf. Sci.* **191**, 288 (1987).  
<sup>16</sup>S. H. Kim, H. L. Meyerheim, J. Barthel, J. Kirschner, J. Seo, and J. S. Kim, *Phys. Rev. B* **71**, 205418 (2005).  
<sup>17</sup>G. Kresse and J. Hafner, *Phys. Rev. B* **47**, 558 (1993).  
<sup>18</sup>G. Kresse and J. Hafner, *Phys. Rev. B* **48**, 13115 (1993).  
<sup>19</sup>G. Kresse and J. Furthmüller, *Comput. Mater. Sci.* **6**, 15 (1996).  
<sup>20</sup>G. Kresse and J. Furthmüller, *Phys. Rev. B* **54**, 11169 (1996).  
<sup>21</sup>J. P. Perdew, J. A. Chevary, S. H. Vosko, K. A. Jackson, M. R. Pederson, D. J. Singh, and C. Fiolhais, *Phys. Rev. B* **46**, 6671 (1992).  
<sup>22</sup>P. E. Blöchl, *Phys. Rev. B* **50**, 17953 (1994).  
<sup>23</sup>G. Kresse and D. Joubert, *Phys. Rev. B* **59**, 1758 (1999).  
<sup>24</sup>M. Methfessel and A. T. Paxton, *Phys. Rev. B* **40**, 3616 (1989).  
<sup>25</sup>A. Lozano, A. Groß, and H. F. Busnengo, *Phys. Chem. Chem. Phys.* **11**, 5814 (2009).  
<sup>26</sup>A. Lozano and H. F. Busnengo (to be published).  
<sup>27</sup>H. F. Busnengo, A. Salin, and W. Dong, *J. Chem. Phys.* **112**, 7641 (2000).  
<sup>28</sup>G. Mills, H. Jónsson, and G. K. Schenter, *Surf. Sci.* **324**, 305 (1995).